

Indirect Torque Control of a Cascaded Brushless Doubly-Fed Induction Generator Operating with Unbalanced Power Grid

Gennadiy Dauksha, Grzegorz Iwanski, *Senior Member, IEEE*

Abstract - This paper describes an indirect torque control algorithm for a cascaded brushless doubly-fed generator (CBDFIG). The control algorithm presented in the paper provides a possibility for CBDFIG to work with an unbalanced power grid applying different strategies: electromagnetic torque oscillations reduction, generated active power oscillation reduction, generated phase currents balancing, sinusoidal control currents under grid imbalance. The proposed control method is based on a cascaded brushless doubly-fed induction generator equivalent model and requires fewer tuning-demanding elements in comparison to classic control methods. The control algorithm presented in the paper was implemented and tested on a CBDFIG machine model in a simulation environment PSIM and on a real physical stand with a cascaded brushless doubly-fed generator.

Keywords - cascaded brushless doubly-fed induction generator, indirect torque control, unbalanced grid.

I. INTRODUCTION

At present, doubly-fed induction generator (DFIG) based power units are a dominating solution in wind energy conversion systems available on the global market [1][2]. The DFIG-based wind power unit is characterized by the lowest capital costs as a result of a relatively low cost of an electrical generator and a partial-sized power converter design [3]. However, its durability strongly depends on regular maintenance since brushes are an indispensable construction feature of this electric machine [4]; the second major problem is grid disturbances and imbalance, which strongly impacts the generator [5]. Due to the significant number of wind generators connected to medium power grids with 2-3% imbalance steady state operation allowed, the problem of generator operation under grid unbalanced conditions is still valid [6].

To eliminate problems with slip-rings, a brushless doubly-fed induction generator (BDFIG) has been invented [7]. Among all types of brushless doubly-fed induction generators, a cascaded brushless doubly-fed induction generator (CBDFIG) is widely described due to construction simplicity and as a consequence – low cost and high durability [8].

Manuscript received; revised; accepted

The work was supported by the statutory funds of Warsaw University of Technology. The authors are with the Institute of Control and Industrial Electronics, Warsaw University of Technology, Warszawa 00-662, Poland (e-mail: iwanski@isep.pw.edu.pl; gennadiy.dauksha@ee.pw.edu.pl).

The CBDFIG-based power unit (Fig. 1) still keeps the classic DFIG advantage - lower capital costs caused by the relatively low cost of partial-sized converter design including passive filters, and increases its durability due to removed slip-rings and brushes [9][10].

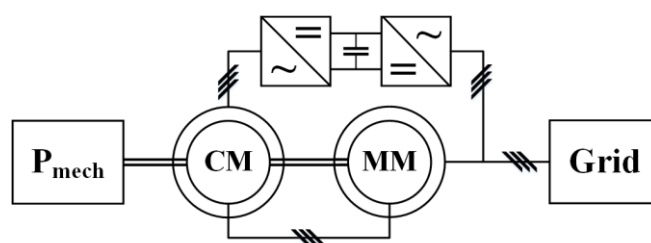


Fig. 1. Scheme of the cascaded brushless doubly-fed induction generator power unit: control machine (CM) and main machine (MM).

As it is similar to DFIG [11], the cascaded brushless doubly-fed generator is susceptible to grid voltage imbalance as well [12]. In contrast to the classic doubly-fed induction generator [13], work of CBDFIG with an unbalanced grid is not well studied.

In [14] and [15], the authors propose modified main stator voltage oriented control algorithms for a stand-alone CBDFIG supplying unbalanced loads. Methods elaborated for stand-alone operation are not suitable for grid operation due to the different task, which is output voltage control in the place of the control of current or power fed to the grid.

In [16], the authors introduce a main stator voltage oriented control with a separate power components regulation path and negative sequence of the main stator current regulation path. The presented algorithm provides the possibility of CBDFIG electromagnetic torque reduction under grid voltage imbalance in order to prevent mechanical stresses of rotating parts. The method proposed in [16] requires decomposition on positive and negative sequence of both main stator voltage and main stator current signals. To achieve this goal, the authors use the DSOGI (Dual Second-Order Generalized Integrator) structure. However, DSOGI accuracy and performance strongly depends on tuning parameters [17]. In combination with tuning parameters of power and current regulators, performance and stability of the method presented in [16] strongly depends on how well regulators and DSOGI structures are tuned, which could be achieved with difficulty due to a high number of tuning dependent terms in the control structure.

In [18], the authors introduce a main stator flux oriented vector control with a separate power components regulation path and the main stator current negative sequence regulation path. Additionally, the control stator regulation path is divided into a positive sequence regulation path and a negative sequence regulation path. The control algorithm proposed in [18] can work under one of the three strategies: generated active power oscillations reduction, generated phase currents balancing, sinusoidal control currents under grid voltage imbalance. The method presented in [18] requires estimation of main stator flux, decomposition of positive and negative sequence grid voltage, main stator current and flux. As a method of decomposition the authors propose a combination of Park's transformation with BSF (Band Stop Filter) tuned on particular harmonics. A major disadvantage of the control method proposed in [18] is the use of BSF for positive and negative decomposition of given signals. Due to construction properties of the digital filters dumping ratio for a particular frequency for a digital filter depends on the filter order and the pass frequency window [19]. For more efficient suppression of the desired frequency it is necessary to raise the order of a filter, though an increase in the digital filter order adversely affects the dynamic response of a filter [20]. In the method proposed in [18], the authors have to deal with the presence of distortions in control signals when better dynamic response is needed, whereas in the case of better signal filtering quality, dynamic deterioration has to be taken into account. Additionally, a large number of tuning dependent structures, such as regulators, negatively influences reaching the desired dynamics and stability of the whole system.

In [21], the authors introduce an improved main stator voltage oriented vector which allows work of CBDFIG with unbalanced grid under one of the four strategies: electromagnetic torque oscillations reduction, generated active power oscillation reduction, generated phase currents balancing, and sinusoidal control currents under grid imbalance. The control algorithm presented in [21] uses a brushless doubly-fed induction generator equivalent model to calculate part of the control current related to the desired main stator negative sequence current. The method presented in [21] requires decomposition of grid voltage on a positive and negative sequence. In the control algorithm proposed in [21] the authors extend a regular main stator voltage oriented control scheme with main stator negative sequence decoupling terms. Basing on a CBDFIG equivalent model in [21], the authors propose calculation of a negative sequence in the control current corresponding to the desired amount of negative sequence in the main stator current according to the desired strategy. The main control path in the method presented in [21] uses a large number of tuning-demanding structures, whereas the negative sequence decoupling path strongly depends on machine parameters.

In [22], the authors present an improved direct power control algorithm for CBDFIG working on an unbalanced grid. The control algorithm proposed in [22] allows to achieve balanced main stator current under grid voltage unbalanced conditions. In order to control p and q power components two hysteresis controllers are used in the control scheme, individual for each power component. In order to achieve the main stator balanced current under grid voltage unbalanced

conditions, in [22] the authors propose injection (to the desired reference values of p and q power components) of specified negative sequence power components corresponding to the main stator balanced current strategy. The algorithm requires decomposition of a positive and negative sequence of grid voltage and main stator current. The control method presented in [22] has a major disadvantage associated with the direct power control scheme using hysteresis controllers – inconstant switching frequency of a power converter. Moreover, hysteresis controllers for better operation require (from data acquisition and the computing unit) work at much higher frequencies in comparison to constant frequency switching algorithms [23]. Additionally, tuning-demanding structures like positive/negative sequence decomposers adversely influence the desired dynamics and stability.

In [24], the authors propose predictive CBDFIG control based on a cascaded brushless doubly-fed induction generator equivalent model. The control scheme proposed in [24] was verified for a symmetrical grid only. The work of the algorithm presented in [24] under grid unbalanced conditions was not performed. The assumed simplifications for finding the relations between the commanded torque and q component of power, and d and q components of current respectively, are valid for symmetrical grid voltage, but cannot be used for asymmetrical grid voltage.

In this paper, the authors propose an indirect torque control method for a cascaded brushless doubly-fed induction generator with the possibility of applying one of the four strategies: electromagnetic torque oscillations reduction, generated active power oscillation reduction, generated phase currents balancing and sinusoidal control currents under grid voltage imbalance. The indirect torque control algorithm presents a method of calculation of the control stator current on the basis of commanded electromagnetic torque T_e^{ref} and reactive power component q_s^{ref} using an equivalent model of a cascaded brushless doubly-fed induction generator.

The control method presented in this paper requires significantly fewer tuning-demanding structures in comparison to the algorithms [16][18][21][22] described above.

Comparing to [16], the control algorithm presented in this paper CBDFIG provides a possibility of applying reduction strategies additional to electromagnetic torque: active power oscillations reduction strategy, balanced main stator current strategy, sinusoidal control current strategy. The control method does not require a positive/negative sequence decomposer, superior power regulators or main stator negative sequence current regulators.

In comparison to [18], indirect torque control for a cascaded brushless doubly-fed induction generator provides electromagnetic torque oscillations reduction target not considered in [18]. Furthermore, lack of the necessity of positive/negative sequence decomposers in the proposed CBDFIG control method eliminates problems with signals filtration presented in [18].

Comparing to [21], the proposed indirect CBDFIG torque control allows to eliminate p and q power components regulators, positive/negative sequence decomposers, which results in significant reduction of dependence on tuning-demanding elements and simplification in reaching the desired dynamics and stability.

In comparison to [22], the CBDFIG control algorithm presented in this paper provides a possibility of applying a main stator current strategy additional to the balanced one: electromagnetic torque reduction strategy, active power oscillations reduction strategy, sinusoidal control current strategy. Moreover, in contrast to the control method presented in [22], indirect torque control ensures constant switching frequency for the CBDFIG power converter connected to the control stator. Absence of superior p and q power component regulators as well as positive/negative decomposing structures facilitates reaching the desired dynamics and stability in a less complicated way in the case of indirect torque control.

A comparison of the CBDFIG predictive control algorithm proposed in [24] with the CBDFIG indirect torque control presented in this paper is performed in chapter IV.

It has to be clearly stated that regardless of the used method designed for unbalanced grid voltage operation conditions of BDFIG, the assumed individual targets can be achieved in steady states, because the method uses the controllers structures which have a high gain for 50Hz or 100Hz (depending on the reference frame used in the control structure). The difference lies in the dynamic behavior, which is the worst when the measured state variables (machine currents) are additionally filtered by second order band pass filters, such as, e.g., SOGI in decomposers. Additional filters in the measurement paths worsen the dynamics of the control plant, because the used filters are additional transfer functions connected in series to the BDFIG first order transfer function. Thus, for the single path controller, the new control plant becomes a third order plant.

II. MODEL OF A CASCADED BRUSHLESS DOUBLY-FED INDUCTION GENERATOR

The cascaded brushless doubly-fed induction generator can be represented as two face-to-face mechanically coupled doubly-fed induction machines [25]: control machine (CM) and main machine (MM) (Fig. 2). Using a well-known DFIG model and assuming electrical circuit symmetry between all phases for the control machine and for the main machine, an equivalent CBDFIG circuit in a grid voltage aligned rotating frame can be built (Fig. 3) [26].

Having an equivalent circuit in a grid voltage vector aligned rotating frame and using dependences for a classic slip-ring doubly-fed induction machine, basic equations describing the cascaded brushless doubly-fed induction generator [26] can be formulated (1a-h).

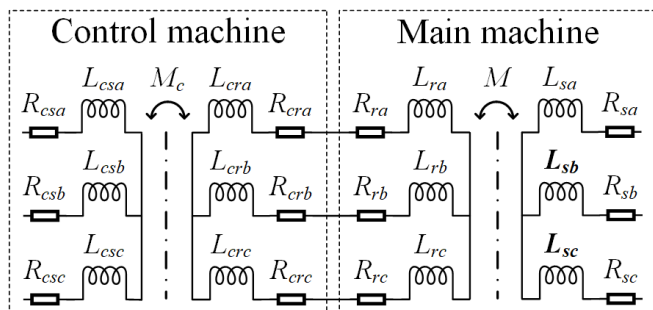


Fig. 2. Cascaded brushless doubly-fed induction generator: control machine (CM) and main machine (MM).

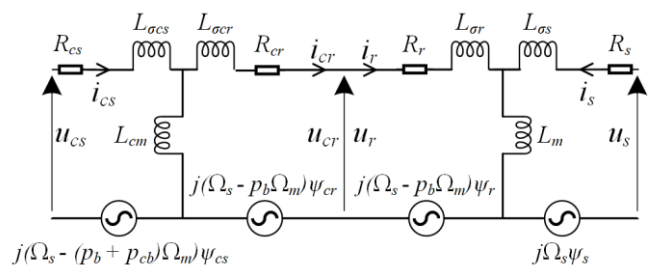


Fig. 3. Cascaded Brushless Doubly-Fed Induction Generator equivalent circuit.

$$u_s = R_s i_s + \frac{d\psi_s}{dt} + j\Omega_s \psi_s \quad (1a)$$

$$u_r = R_r i_r + \frac{d\psi_r}{dt} + j(\Omega_s - p_b \Omega_m) \psi_r \quad (1b)$$

$$u_{cs} = R_{cs} i_{cs} + \frac{d\psi_{cs}}{dt} + j(\Omega_s - (p_b + p_{cb})\Omega_m) \psi_{cs} \quad (1c)$$

$$u_{cr} = R_{cr} i_{cr} + \frac{d\psi_{cr}}{dt} + j(\Omega_s - p_b \Omega_m) \psi_{cr} \quad (1d)$$

$$\psi_s = L_s i_s + L_m i_r \quad (1e)$$

$$\psi_r = L_m i_s + L_r i_r \quad (1f)$$

$$\psi_{cs} = L_{cs} i_{cs} + L_{cm} i_{cr} \quad (1g)$$

$$\psi_{cr} = L_{cm} i_{cs} + L_{cr} i_{cr} \quad (1h)$$

Due to direct electric coupling between the main machine and the control machine rotor circuits and taking into account (according to the defined CBDFIG equivalent circuit (Fig. 3)) opposite directions of a rotor current for the main machine and the control machine, the following statements are correct for the cascaded brushless doubly-fed induction machine [26]:

$$u_r = u_{cr} \quad (2a)$$

$$i_r = -i_{cr} \quad (2b)$$

Taking into account negligible voltage drops on rotor resistances for both the main machine and the control machine it can be assumed that rotor magnetic fluxes depend mainly on the rotor voltage of the main machine and the control machine respectively (Fig. 3). Therefore the relation between the main machine rotor magnetic flux and the control machine rotor magnetic flux can be formulated as follows [26]:

$$\psi_r \approx \psi_{cr} \quad (2c)$$

Equations (1d), (1g) and (1h) can be rewritten using (2b) as follows [26]:

$$u_r \approx -R_{cr} i_r + \frac{d\psi_r}{dt} + j(\Omega_s - p_b \Omega_m) \psi_r \quad (3a)$$

$$\psi_{cs} = L_{cs} i_{cs} - L_{cm} i_r \quad (3b)$$

$$\psi_r \approx L_{cm} i_{cs} - L_{cr} i_r \quad (3c)$$

Finally, substituting (1d), (1g) and (1h) with (3a), (3b) and (3c) respectively, and then subtracting (3a) from (1b), and (3c) from (1f), equations describing the cascaded brushless doubly-fed induction machine equivalent circuit (Fig. 3) could be formulated as follows [26]:

$$u_s = R_s i_s + \frac{d\psi_s}{dt} + j\Omega_s \psi_s \quad (4a)$$

$$0 \approx (R_r + R_{cr}) i_r \quad (4b)$$

$$u_{cs} = R_{cs}i_{cs} + \frac{d\psi_{cs}}{dt} + j(\Omega_s - (p_b + p_{cb})\Omega_m)\psi_{cs} \quad (4c)$$

$$\psi_s = L_s i_s + L_m i_r \quad (4d)$$

$$0 \approx (L_r + L_{cr})i_r + L_m i_s - L_{cm}i_{cs} \quad (4e)$$

$$\psi_{cs} = L_{cs}i_{cs} + L_{cm}i_{cr} \quad (4f)$$

Treating the CBDFIG model as two mechanically coupled machines according to the scheme from Fig. 3, its electromagnetic torque equations can be formulated as follows [27]:

$$T_{me} = 1.5p_b(\psi_{sa}i_{s\beta} - \psi_{s\beta}i_{sa}) = 1.5p_b(\psi_{r\beta}i_{r\alpha} - \psi_{r\alpha}i_{r\beta}) \quad (5a)$$

$$T_{ce} = 1.5p_{cb}(\psi_{cs\alpha}i_{cs\beta} - \psi_{cs\beta}i_{cs\alpha}) = 1.5p_{cb}(\psi_{cr\beta}i_{cr\alpha} - \psi_{cr\alpha}i_{cr\beta}) \quad (5b)$$

Using (2b) and (2c), equation (5b) can be rewritten:

$$T_{ce} = 1.5p_{cb}(\psi_{cs\alpha}i_{cs\beta} - \psi_{cs\beta}i_{cs\alpha}) \approx -1.5p_{cb}(\psi_{r\beta}i_{r\alpha} - \psi_{r\alpha}i_{r\beta}) \quad (5c)$$

Equations (5a) and (5c) derive the following relationship (5d) between the main machine electromagnetic torque and the control machine electromagnetic torque:

$$\frac{T_{me}}{p_b} \approx -\frac{T_{ce}}{p_{cb}} \quad (5d)$$

In turn, the total torque of CBDIG, taking into account opposite rotation of the control machine in relation to the main machine due to face-to-face connection and (5d), can be described by the following equations:

$$T_e = T_{me} - T_{ce} \quad (5e)$$

$$T_e \approx \left(\frac{p_b + p_{cb}}{p_b}\right)T_{me} \quad (5f)$$

$$T_e \approx -\left(\frac{p_b + p_{cb}}{p_{cb}}\right)T_{ce} \quad (5g)$$

It should be noted that due to relation (5d) between the main machine and the control machine, disturbances or oscillations in T_{me} automatically provide disturbances or oscillations in T_{ce} and vice-versa oscillations. Simultaneously cancellation of oscillations in T_{me} provides oscillations cancellation in T_{ce} and resulting total torque T_e oscillations cancellation.

Applying instantaneous power theory for multiphase electric circuits, instantaneous power produced by CBDFIG could be defined as a sum of instantaneous powers produced by the main machine and the control machine respectively [28]:

$$p_s = 1.5(u_{sa}i_{s\alpha} + u_{s\beta}i_{s\beta}) \quad (6a)$$

$$q_s = 1.5(u_{s\beta}i_{s\alpha} - u_{sa}i_{s\beta}) \quad (6b)$$

$$p_{cs} = 1.5(u_{cs\alpha}i_{cs\alpha} + u_{cs\beta}i_{cs\beta}) \quad (6c)$$

$$q_{cs} = 1.5(u_{cs\beta}i_{cs\alpha} - u_{cs\alpha}i_{cs\beta}) \quad (6d)$$

$$p = p_s + p_{cs} \quad (6e)$$

$$q = q_s + q_{cs} \quad (6f)$$

III. INDIRECT TORQUE CONTROL ALGORITHM FOR CBDFIG WORKING WITH UNBALANCED GRID

Under grid voltage imbalance, two mutually exclusive boundary control strategies can be implemented: the instantaneous p_s power component oscillations cancellation

strategy and the electromagnetic torque oscillations cancellation strategy. Additionally, two strategies can be formulated: main stator phase current balancing, which is a compromise between the two strategies mentioned above, and sinusoidal control currents for the control machine [21].

The instantaneous p_s power component oscillations cancellation strategy allows to achieve an equal number of active power components generated at each phase of the main machine by generating higher currents in weaker phases. This strategy is helpful for an unbalanced grid, but increases electromagnetic torque oscillations [18] in relation to the other strategies.

In contrast to the p_s component oscillations cancellation strategy, the electromagnetic torque oscillations cancellation strategy provides lower currents in weaker phases of the main machine stator in order to decrease electromagnetic torque oscillations caused by grid voltage imbalance. In such case, the amount of active power flowing to the grid is unequal for each phase, there is more active power in stronger phases and less power in weaker phases [21].

The main machine stator phase currents balancing strategy can be treated as a compromise between the main machine stator p power component oscillations cancellation strategy and the electromagnetic torque oscillations cancellation strategy. Performing the main stator phase current balancing strategy allows to reduce electromagnetic torque oscillations by half in comparison to the p_s power component oscillations cancellation strategy and reduces p_s power component oscillations by half in comparison to the electromagnetic torque oscillations cancellation strategy at the same time [22]. Similar oscillations of main machine stator instantaneous power components and electromagnetic torque can be achieved with the fourth strategy, which is sinusoidal balanced control stator current.

The control strategies for the CBDFIG grid formulated above are a minor goal for the control algorithm, which results in increasing generated power quality under grid unbalanced conditions. The main goal which the control algorithm has to achieve is generation of the desired amount of active and reactive power. Active power P_s of the main machine stator is an average value of the p_s component of instantaneous power. Although there are several power theories related to reactive power, the reactive power can be calculated with the average value of the q component of instantaneous power, with a minor approximation error independently of the power theory used. The proposed indirect torque control algorithm requires the commanded value of electromagnetic torque. The reference value of the main machine electromagnetic torque can be calculated using commanded active power (7). It should be noted that this way the average value of torque can be found. However, in the proposed method, the average value of torque is referenced, whereas separate targets will be achieved by adequate calculations of the control machine stator current vector components.

$$T_{me}^{ref} = p_b \left(\frac{P_s^{ref}}{\Omega_s} \right) \quad (7)$$

Having the reference main machine electromagnetic torque T_{me}^{ref} and the main machine reference q component of instantaneous power q_s^{ref} , we are able to calculate the desired

main stator current using a term of (5a) and (6b) referenced to the main machine:

$$i_{s\alpha}^{ref} = \frac{2}{3} \left(\frac{u_{s\alpha} \frac{T_{me}^{ref}}{p_b} + \psi_{s\alpha} q_s^{ref}}{u_{s\beta} \psi_{s\alpha} - u_{s\alpha} \psi_{s\beta}} \right) \quad (8a)$$

$$i_{s\beta}^{ref} = \frac{2}{3} \left(\frac{u_{s\beta} \frac{T_{me}^{ref}}{p_b} + \psi_{s\beta} q_s^{ref}}{u_{s\beta} \psi_{s\alpha} - u_{s\alpha} \psi_{s\beta}} \right) \quad (8b)$$

To obtain the main stator reference current, we need to know the main stator flux. It can be obtained from (4a) by integration of the main stator electromotive force:

$$\psi_{s\alpha} = \int (u_{s\alpha} - R_s i_{s\alpha}) dt \quad (9a)$$

$$\psi_{s\beta} = \int (u_{s\beta} - R_s i_{s\beta}) dt \quad (9b)$$

In practice, realization of pure integration is hardly possible due to parasitic dc component presence in the measured signals, which results in integrators output signals rising to infinity. Assuming that grid frequency is almost stable and equals f_s , pure integration (9) could be replaced by a second-order low pass filter with cut-off frequency equal to f_s . In such case a phase-shift provided by the filter is -90 degrees for f_s harmonic in the signal. Assuming that the main stator electromotive force frequency equals grid frequency f_s , applying on the main stator electromotive force, a second-order low pass filter with the same cut-off frequency gives us the value of the stator electromotive force shifted by -90 degrees like for pure integration. The received shifted main stator electromotive force signal has to be amplified by 3db (multiplied by $k \approx 1.4$) in order to compensate for a low pass filter 3db attenuation at f_s cut-off frequency. Finally, division by grid pulsation Ω_s , achieved above the shifted main machine stator electromotive force gives the main machine stator flux (Fig. 4):

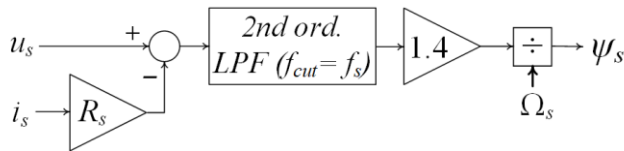


Fig. 4. Main machine stator flux estimator based on the second-order low pass filter.

Based on the obtained above stator current reference and stator flux values we are able to define the corresponding reference rotor current using (4d):

$$i_{r\alpha}^{ref} = \left(\frac{\psi_{s\alpha} - L_s i_{s\alpha}^{ref}}{L_m} \right) \eta_{SR} \quad (10a)$$

$$i_{r\beta}^{ref} = \left(\frac{\psi_{s\beta} - L_s i_{s\beta}^{ref}}{L_m} \right) \eta_{SR} \quad (10b)$$

Stator current reference calculated from (8) and rotor current reference values calculated from (10) allow to determine the control-side stator current using (4e):

$$i_{cs\alpha}^{ref} = \left(\frac{(L_r + L_{cr}) i_{r\alpha}^{ref} - \eta_{SR} L_m i_{s\alpha}^{ref}}{\eta_{CSR} L_{cm}} \right) \quad (11a)$$

$$i_{cs\beta}^{ref} = \left(\frac{(L_r + L_{cr}) i_{r\beta}^{ref} - \eta_{SR} L_m i_{s\beta}^{ref}}{\eta_{CSR} L_{cm}} \right) \quad (11b)$$

Calculated from (11), the control machine reference current is naturally placed in a grid voltage stationary $\alpha\beta$ frame. To receive the desired values of the control machine current, proportional-resonant PR regulators are used, where resonant pulsation is set equal to grid voltage pulsation [30]. To make control machine current regulators work correctly, the measured control machine current has to be transformed from the control machine stationary $\alpha\beta$ frame to the grid voltage stationary $\alpha\beta$ frame using Park rotation transformation, whereas output values obtained from proportional-resonant current regulators have to be transformed back using the inverse Park transformation to the control machine stationary $\alpha\beta$ frame.

The control method presented above ensures the desired amount of active (average value of the p component of instantaneous power) and reactive (average value of the q component instantaneous power) power with the electromagnetic torque oscillations reduction strategy under grid voltage unbalanced conditions. In this case, the main stator reference current calculated from (8) has the same asymmetry as grid voltage, which results in electromagnetic torque oscillation reduction. To apply another strategy, active power component oscillations reduction, the calculated main stator reference current should have opposite asymmetry to grid voltage.

An oppositely unbalanced grid voltage could be calculated from the main machine stator flux (Fig. 4) with the following equations:

$$u'_{s\alpha} = (R_s i_{s\alpha} - \psi_{s\beta} \Omega_s) \quad (12a)$$

$$u'_{s\beta} = (R_s i_{s\beta} + \psi_{s\alpha} \Omega_s) \quad (12b)$$

Similarly, unbalanced main stator flux can be obtained with the following equations:

$$\psi'_{s\alpha} = \left(\frac{u_{s\beta} - R_s i_{s\beta}}{\Omega_s} \right) \quad (13a)$$

$$\psi'_{s\beta} = - \left(\frac{u_{s\alpha} - R_s i_{s\alpha}}{\Omega_s} \right) \quad (13b)$$

Having the main reference machine electromagnetic torque, main machine reference reactive power, oppositely unbalanced grid voltage and oppositely unbalanced main stator flux we are able to calculate the main stator current ensuring active power component oscillations reduction from (5a) and (6b):

$$i'_{s\alpha}{}^{ref} = \frac{2}{3} \left(\frac{u'_{s\alpha} \frac{T_{me}^{ref}}{p_b} + \psi'_{s\alpha} q_s^{ref}}{u'_{s\beta} \psi'_{s\alpha} - u'_{s\alpha} \psi'_{s\beta}} \right) \quad (14a)$$

$$i'_{s\beta}{}^{ref} = \frac{2}{3} \left(\frac{u'_{s\beta} \frac{T_{me}^{ref}}{p_b} + \psi'_{s\beta} q_s^{ref}}{u'_{s\beta} \psi'_{s\alpha} - u'_{s\alpha} \psi'_{s\beta}} \right) \quad (14b)$$

The reference control machine stator current for this target (non-oscillating p power component) is calculated analogously to the calculations made for the torque oscillations cancellation target using equations (10) and (11), in which instead of i_{sa}^{ref} and $i_{s\beta}^{ref}$, new variables $i_{sa}^{\prime ref}$ and $i_{s\beta}^{\prime ref}$ are used.

Obtained from (8) and (14), the reference values of the main stator current present two mutually exclusive control strategies: active power component oscillations reduction strategy and electromagnetic torque oscillations reduction strategy. In order to achieve a balanced main stator current the positive sequence component has to be extracted from the reference values of the main stator current mentioned above. Basing on the fact that the reference values calculated from (8) and (14) have opposite imbalance, a positive component of the desired main stator current can be achieved as follows.

$$i_{sa}^{+ref} = \left(\frac{i_{sa}^{ref} + i_{sa}^{\prime ref}}{2} \right) \quad (15a)$$

$$i_{s\beta}^{+ref} = \left(\frac{i_{s\beta}^{ref} + i_{s\beta}^{\prime ref}}{2} \right) \quad (15b)$$

Finally, having positive sequence components of the desired main stator current and oppositely unbalanced main stator flux, the fourth strategy, sinusoidal control currents can be realized using (10), (11), (13) and (15):

$$i_{ra}^{+ref} = \left(\frac{\left(\frac{\psi_{sa} + \psi'_{sa}}{2} \right) - L_s i_{sa}^{+ref}}{L_m} \right) \eta_{SR} \quad (16a)$$

$$i_{r\beta}^{+ref} = \left(\frac{\left(\frac{\psi_{s\beta} + \psi'_{s\beta}}{2} \right) - L_s i_{s\beta}^{+ref}}{L_m} \right) \eta_{SR} \quad (16b)$$

$$i_{csa}^{+ref} = \left(\frac{(L_r + L_{cr}) i_{ra}^{+ref} - \eta_{SR} L_m i_{sa}^{+ref}}{\eta_{CSR} L_{cm}} \right) \quad (16c)$$

$$i_{cs\beta}^{+ref} = \left(\frac{(L_r + L_{cr}) i_{r\beta}^{+ref} - \eta_{SR} L_m i_{s\beta}^{+ref}}{\eta_{CSR} L_{cm}} \right) \quad (16d)$$

The control method presented above ensures generation of the desired amount of p and q components of the main machine stator instantaneous power for a cascaded brushless doubly-fed induction generator and gives the possibility of applying one of the four strategies: electromagnetic torque oscillations reduction, generated active power oscillation reduction, generated phase currents balancing, sinusoidal control currents under grid voltage imbalance. Additionally, using (4a) and (4f) we are able to provide additional terms for partial compensation of couplings between control paths:

$$\psi_{csa}^{ref} = \left(L_{cs} i_{csa}^{ref} - \frac{L_{cm} i_{ra}^{ref}}{\eta_{CSR}} \right) \quad (17a)$$

$$\psi_{cs\beta}^{ref} = \left(L_{cs} i_{cs\beta}^{ref} - \frac{L_{cm} i_{r\beta}^{ref}}{\eta_{CSR}} \right) \quad (17b)$$

$$\Delta u_{sa} = \left(R_{cs} i_{csa}^{ref} - (\Omega_s - (p_b + p_{cb}) \Omega_m) \psi_{cs\beta}^{ref} \right) \quad (17c)$$

$$\Delta u_{s\beta} = \left(R_{cs} i_{cs\beta}^{ref} + (\Omega_s - (p_b + p_{cb}) \Omega_m) \psi_{csa}^{ref} \right) \quad (17d)$$

The scheme of indirect torque control for a cascaded brushless doubly-fed induction generator with the possibility of electromagnetic torque oscillations reduction, generated active power oscillations reduction, stator phase current balancing, sinusoidal control currents for unbalanced grid voltage is shown in Fig. 5.

IV. SIMULATION TESTS OF INDIRECT CBDFIG TORQUE CONTROL

Verification of the indirect torque control algorithm, presented above, was performed for the cascaded brushless doubly-fed induction generator model (Tab. 1) implemented in a PSIM simulation environment. The simulated CBDFIG is working with an unbalanced grid (20% of grid voltage imbalance), power converter switching frequency set at 5kHz, settings of both (α component and β component) proportional-resonant (PR) regulators are manually adjusted and equal: $k_p=1$ (proportional part), $k_{res}=100$ (resonant part), $\Omega_s=314.1592$ rad/s (resonant frequency 50Hz), $\Omega_{cut}=15.7$ rad/s (cut-off frequency 2.5Hz, pass-band 47.5-52.5Hz), regulators operate on normalized (per unit) signal values.

Waveforms obtained from the simulation of a cascaded brushless doubly-fed induction generator (Tab. 1) controlled by the indirect torque control algorithm at constant angular speed (1200 rpm) are shown in Fig. 6. As it can be observed, the implemented control algorithm ensures proper work of CBDFIG under unbalanced grid voltage conditions and provides a possibility for realization of one of the four strategies. The first realized strategy, electromagnetic torque oscillations reduction, ensures attenuation of electromagnetic torque and reactive power oscillations. On the other hand, under the electromagnetic torque oscillations reduction strategy, the generator delivers less power to the weaker phase, which impacts generated active power oscillations. The second strategy – stator phase currents balancing – ensures main stator symmetrical phase currents of a cascaded brushless doubly-fed induction generator working with an unbalanced grid. Under this strategy, we obtain partial reduction of electromagnetic torque oscillations and partial reduction of generated active power oscillations. The third strategy, generated active power oscillations reduction, ensures opposite asymmetry of stator currents. This strategy is helpful for unbalanced grid since it delivers more current in a phase with lower voltage which impacts grid voltage balancing. On the other hand, opposite asymmetry of stator currents increases electromagnetic torque oscillations which are harmful for mechanical parts of CBDFIG. The fourth strategy – control machine sinusoidal phase currents – can be helpful to prevent exceeding the maximum value of phase current for the control-side converter and control machine under grid voltage imbalance.

Fig. 7 shows waveforms for the indirect CBDFIG torque control algorithm in the case of reference power changing and torque oscillations reduction strategy under grid voltage imbalance at constant mechanical angular speed (1200 rpm). In Fig. 7, we can see a good dynamic response of the system due to small employment of tuning-demanding structures in the proposed control algorithm which influences short transient states and good dynamics of the closed loop system.

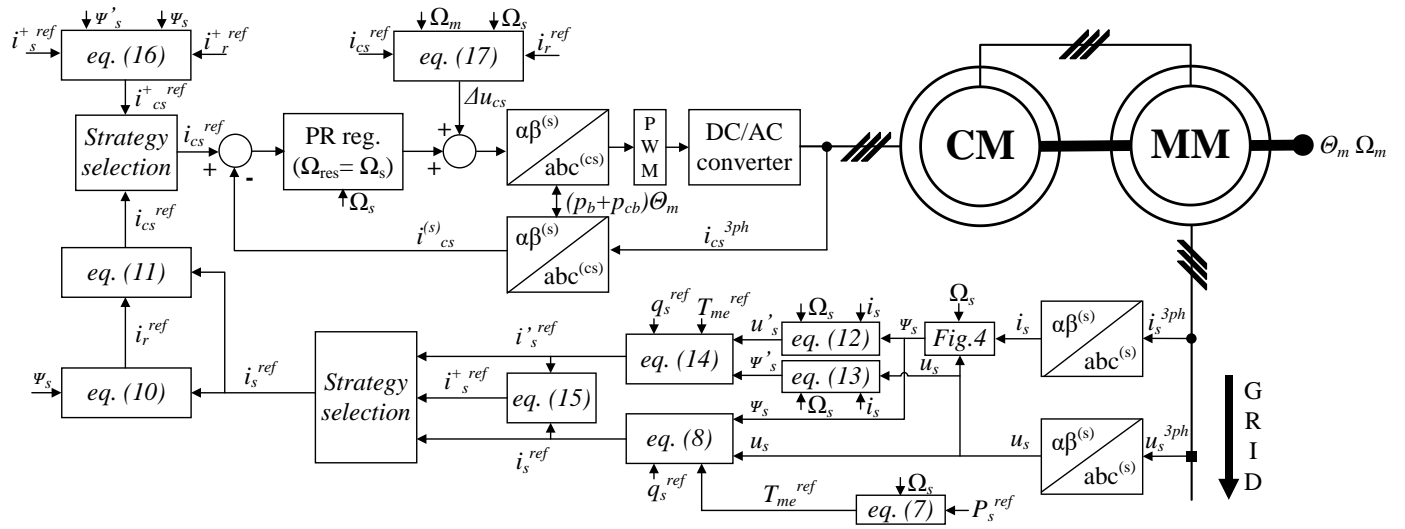


Fig. 5. CBDFIG indirect torque control algorithm block diagram.

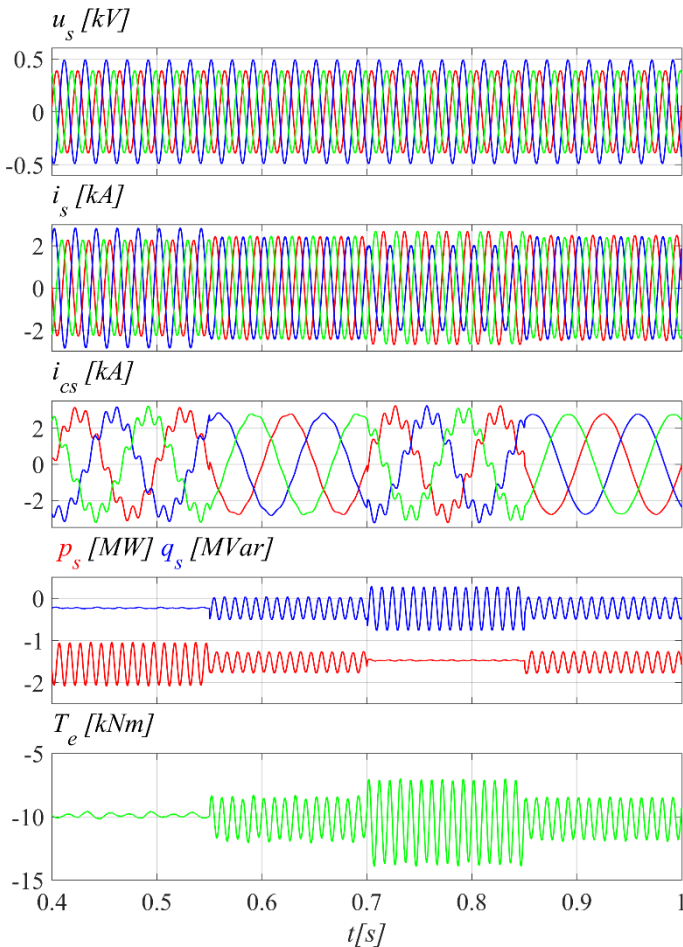


Fig. 6. Grid phase voltages u_{sa}, u_{sb}, u_{sc} ; main stator phase currents i_{sa}, i_{sb}, i_{sc} ; control stator phase currents $i_{csa}, i_{csb}, i_{csc}$; active p_s and reactive q_s power components, electromagnetic torque T_e , for indirect CBDFIG torque control at grid voltage imbalance and electromagnetic torque oscillation reduction, main stator current balancing, active power oscillations reduction, control machine sinusoidal current strategies.

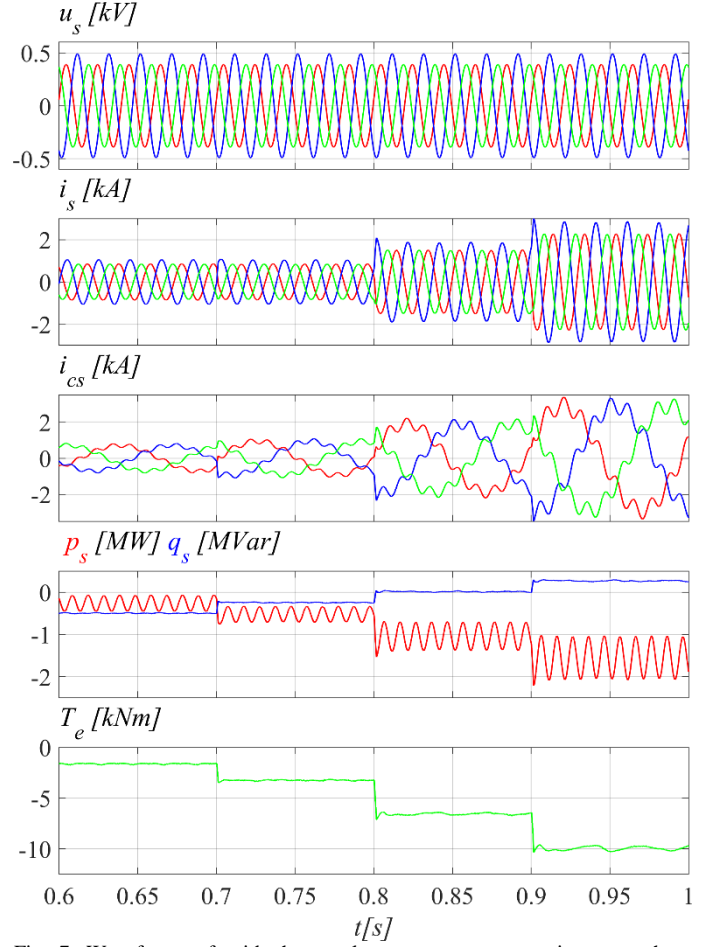


Fig. 7. Waveforms of grid phase voltages u_{sa}, u_{sb}, u_{sc} ; main stator phase currents i_{sa}, i_{sb}, i_{sc} ; control stator phase currents $i_{csa}, i_{csb}, i_{csc}$; p_s and q_s power components; electromagnetic torque T_e , for indirect torque control at reference power change transients and torque oscillation cancellation strategy.

Fig. 8 shows waveforms for the indirect CBDFIG torque control algorithm in the case of linear mechanical angular speed (from 1000 rpm up to 1800 rpm) changing, constant power generation (constant average value of p_s component) and torque oscillations reduction strategy under grid voltage imbalance. In Fig. 8, we can see control current base frequency change as a result of mechanical angular speed changing in order to hold the produced electromagnetic torque and related power at the desired level.

Fig. 9-10 show transient waveforms for 20% grid voltage imbalance for CBDFIG indirect torque control with applied balanced control machine current strategy (Fig. 9) and CBDFIG predictive control described in [24] (Fig. 10), at constant (1200 rpm) mechanical speed. Balanced control machine current has been chosen from among analyzed targets of proposed indirect torque control method, because torque oscillations during sag are the closest to results obtained by method from [24].

It is shown in Fig. 10 that the CBDFIG predictive control [24] algorithm under grid voltage imbalance conditions derives control machine current distorted in a way resulting non-sinusoidal main machine current, therefore none of the discussed above targets for unbalanced grid connection operation is met. CBDFIG main machine indirect torque control is able to derive not only balanced control machine current under grid voltage imbalance (Fig. 9) but control machine current distorted in a way resulting application of one of three more strategies: electromagnetic torque oscillations reduction, balanced main machine current and p power component oscillations reduction respectively (Fig. 6).

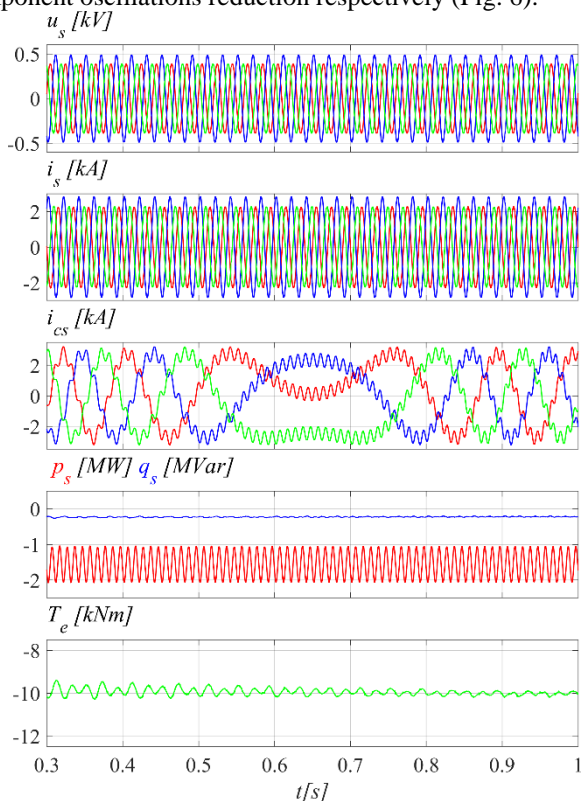


Fig. 8. Waveforms of grid phase voltages u_{sa} , u_{sb} , u_{sc} ; main stator phase currents i_{sa} , i_{sb} , i_{sc} ; control stator phase currents i_{csa} , i_{csb} , i_{csc} ; p_s and q_s power components; electromagnetic torque T_e , for indirect torque control at mechanical angular speed linear change under torque oscillation cancellation strategy.

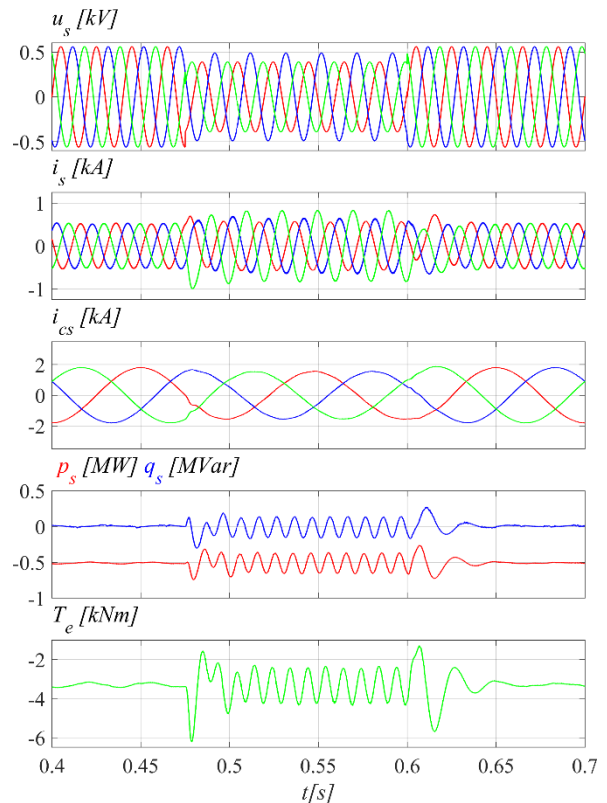


Fig. 9. Waveforms of grid phase voltages u_{sa} , u_{sb} , u_{sc} ; main stator phase currents i_{sa} , i_{sb} , i_{sc} ; control stator phase currents i_{csa} , i_{csb} , i_{csc} ; p_s and q_s power components; electromagnetic torque T_e , for grid voltage imbalance transient under balanced control current strategy.

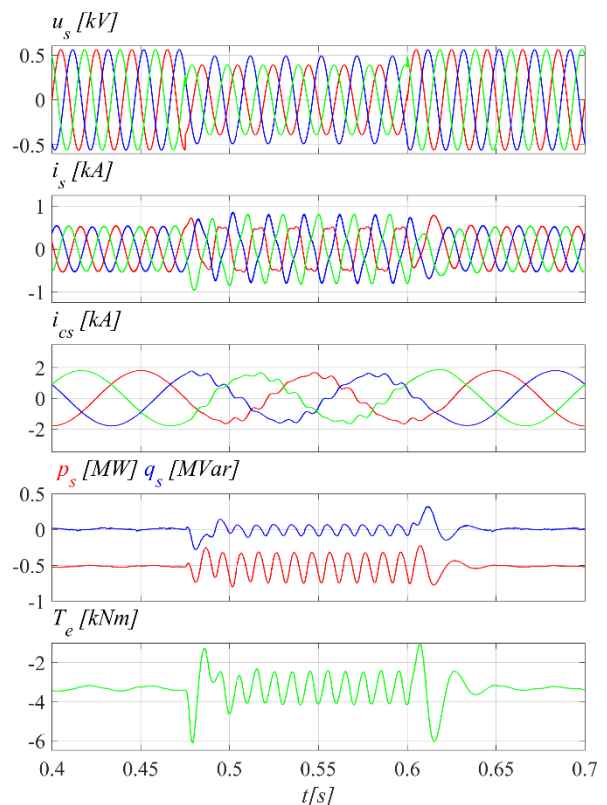


Fig. 10. CBDFIG predictive torque control [24] waveforms of grid phase voltages u_{sa} , u_{sb} , u_{sc} ; main stator phase currents i_{sa} , i_{sb} , i_{sc} ; control stator phase currents i_{csa} , i_{csb} , i_{csc} ; p_s and q_s power components; electromagnetic torque T_e , for grid voltage imbalance transient.

V. IMPLEMENTATION OF INDIRECT TORQUE CONTROL OF CBDFIG

Verification of the control algorithm presented in this paper was performed on a real stand with two slip-ring doubly-fed induction machines, the parameters of which are provided in the Appendix (Tab. 2), connected in a way corresponding to the cascaded brushless doubly-fed induction generator (Fig. 11).

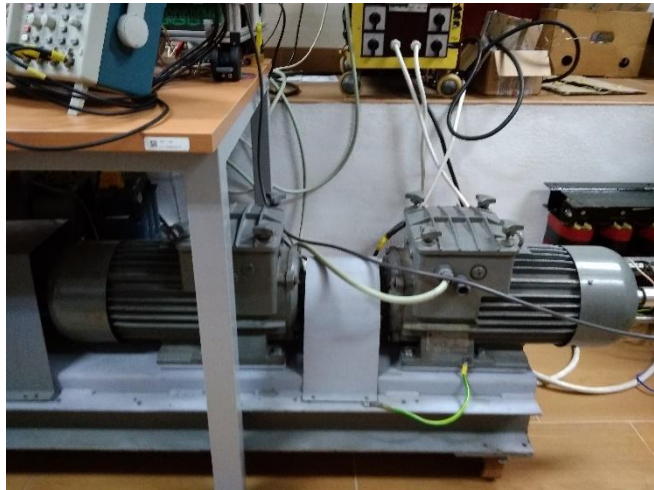


Fig. 11. Slip-ring doubly-fed induction machines connected in a way corresponding to the cascaded brushless doubly-fed induction generator.

The control machine supplied by a power converter worked at 4kHz switching frequency, the settings of both (α component and β component) proportional-resonant (PR) regulators are manually adjusted and equal: $k_p=2.5$ (proportional part), $k_{res}=250$ (resonant part), $\Omega_s=314.1592$ rad/s (resonant frequency 50Hz), $\Omega_{cut}=15.7$ rad/s (cut-off frequency 2.5Hz, pass-band 47.5-52.5Hz), regulators operate on normalized (per unit) signal values.

Fig. 12 – Fig. 15 present grid phase voltages, main machine phase stator currents, control machine phase stator currents, p and q components of the main machine stator power and electromagnetic torque under: electromagnetic torque oscillations cancellation strategy (Fig. 12); generated main machine stator phase currents balancing strategy (Fig. 13); generated active power oscillations reduction strategy (Fig. 14); sinusoidal control machine stator currents strategy (Fig. 15) under grid voltage imbalance. In Fig. 12, we can observe absence of oscillations of electromagnetic torque and the q component of power as a result of grid voltage and main stator current imbalance correspondence. The opposite strategy, active power oscillations cancellation strategy (Fig. 14), produces oppositely unbalanced main stator current resulting in, on the one hand, active power oscillations attenuation and electromagnetic torque oscillations magnification on the other. Strategies presented in Fig. 13 and Fig. 15 provide balanced main machine currents and sinusoidal control machine currents, respectively.

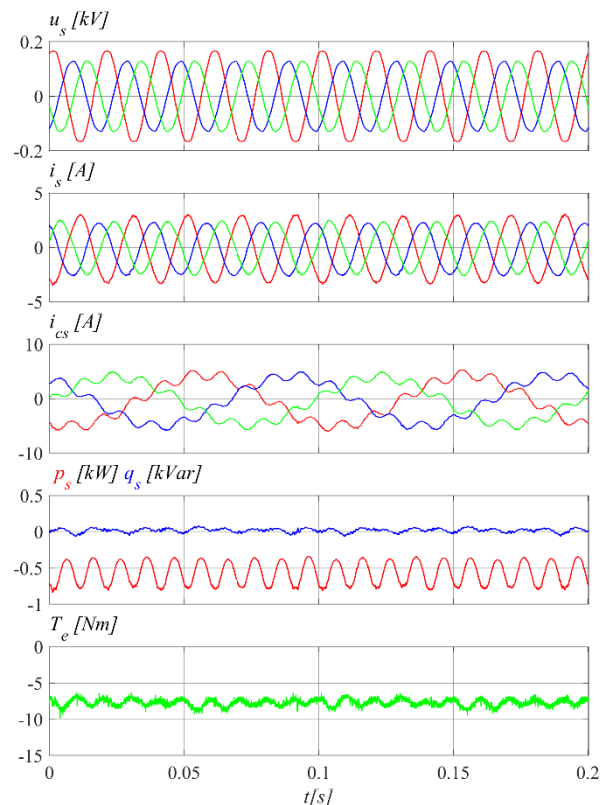


Fig. 12. Grid phase voltages u_{sa} , u_{sb} , u_{sc} ; main stator phase currents i_{sa} , i_{sb} , i_{sc} ; control stator phase currents i_{csa} , i_{csb} , i_{csc} ; p_s and q_s power components, electromagnetic torque T_e , for indirect torque control at grid voltage imbalance and electromagnetic torque oscillation cancellation strategy.

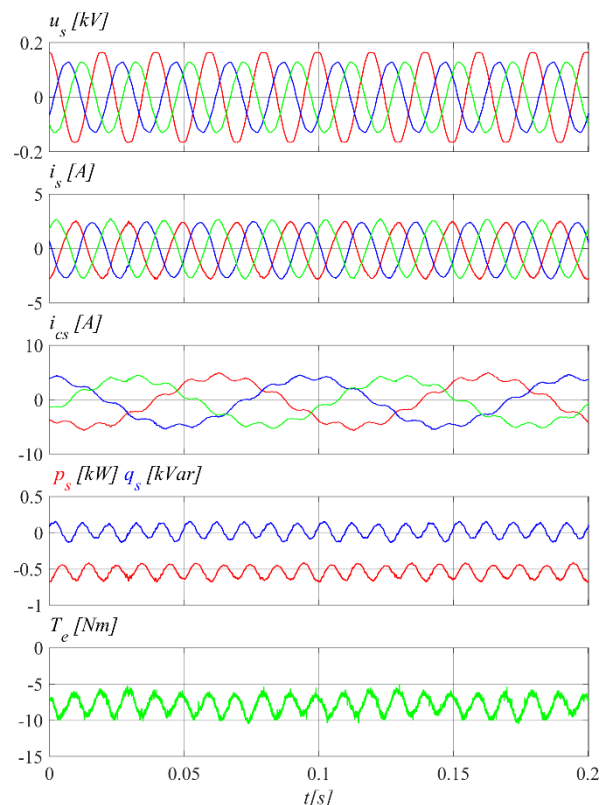


Fig. 13. Grid phase voltages u_{sa} , u_{sb} , u_{sc} ; main stator phase currents i_{sa} , i_{sb} , i_{sc} ; control stator phase currents i_{csa} , i_{csb} , i_{csc} ; p_s and q_s power components, electromagnetic torque T_e , for indirect torque control at grid voltage imbalance and main stator current balancing strategy.

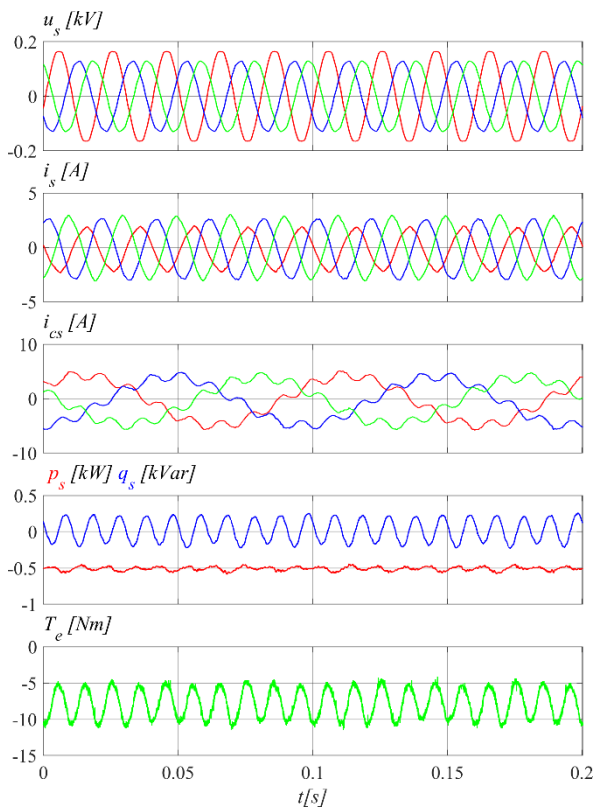


Fig. 14. Grid phase voltages u_{sa} , u_{sb} , u_{sc} ; main stator phase currents i_{sa} , i_{sb} , i_{sc} ; control stator phase currents i_{csa} , i_{csb} , i_{csc} ; p_s and q_s power components, electromagnetic torque T_e , for indirect torque control at grid voltage imbalance and active power oscillations reduction strategy.

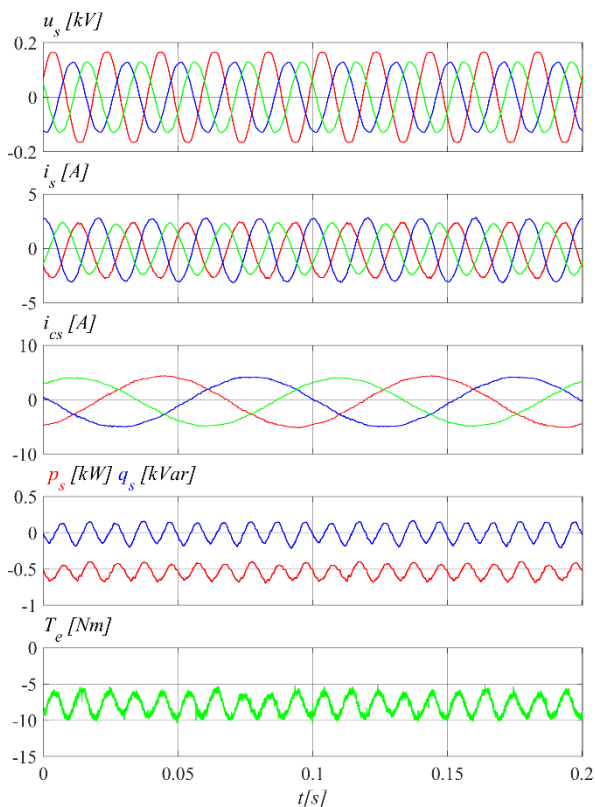


Fig. 15. Grid phase voltages u_{sa} , u_{sb} , u_{sc} ; main stator phase currents i_{sa} , i_{sb} , i_{sc} ; control stator phase currents i_{csa} , i_{csb} , i_{csc} ; p_s and q_s power components, electromagnetic torque T_e , for indirect torque control at grid voltage imbalance and control stator sinusoidal current strategy.

Fig. 16 shows dynamic behavior of a system at reference p and q power components step change. The observed waveforms present the ability of the control system to change generated power in a short time. Good dynamic provided by the indirect torque control algorithm is the result of a smaller number of tuning-demanding structures in comparison to the classic cascaded brushless doubly-fed induction generator control algorithms.

Fig. 17 shows waveforms for the indirect CBDFIG torque control algorithm in the case of linear mechanical angular speed (from 500 rpm up to 700 rpm) changing, constant power generation and torque oscillations reduction strategy under grid voltage imbalance. In Fig. 17, we can see control current base frequency change as a result of mechanical angular speed changing in order to hold the produced electromagnetic torque and power related with it at the desired level.

Fig. 18 and Fig. 19 show dynamic responses of a system under instant grid voltage imbalance and electromagnetic torque oscillations reduction strategy. It can be seen in Fig. 18 and Fig. 19 that transient states of a system in the case of applied grid voltage imbalance (Fig. 18) and in the case of grid voltage recovery (Fig. 19) are very short due to relatively high grid impedance. Performance of a control system equipped with indirect CBDFIG torque control is good enough to be effective in short grid imbalance disturbances.

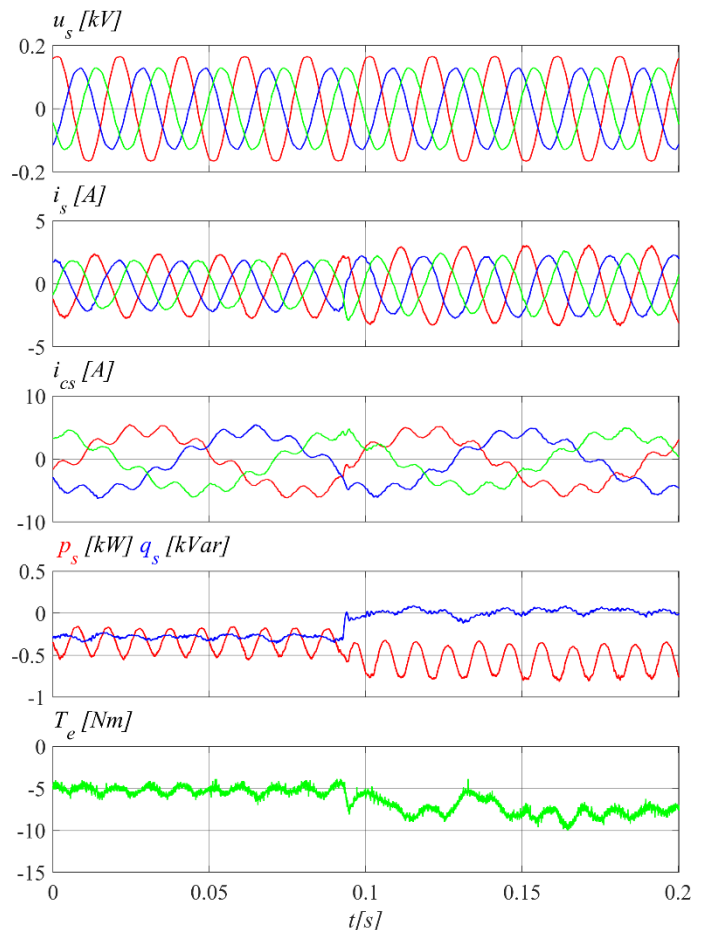


Fig. 16. Grid phase voltages u_{sa} , u_{sb} , u_{sc} ; main stator phase currents i_{sa} , i_{sb} , i_{sc} ; control stator phase currents i_{csa} , i_{csb} , i_{csc} ; active p_s and reactive q_s power components, electromagnetic torque T_e , for indirect torque control at reference power changing under electromagnetic torque oscillation reduction strategy.

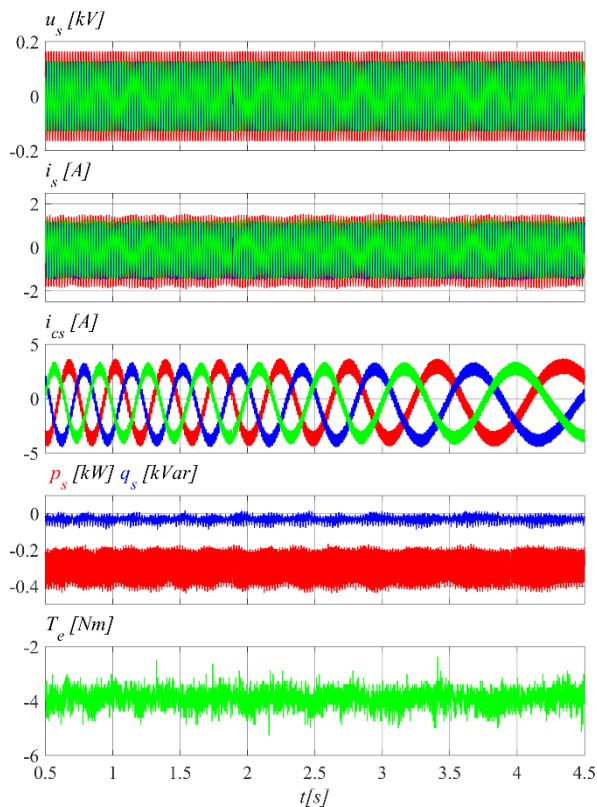


Fig. 17. Grid phase voltages u_{sa} , u_{sb} , u_{sc} ; main stator phase currents i_{sa} , i_{sb} , i_{sc} ; control stator phase currents i_{csa} , i_{csb} , i_{csc} ; active p_s and reactive q_s power components, electromagnetic torque T_e , for indirect torque control at mechanical angular speed linear change under torque oscillation cancellation strategy.

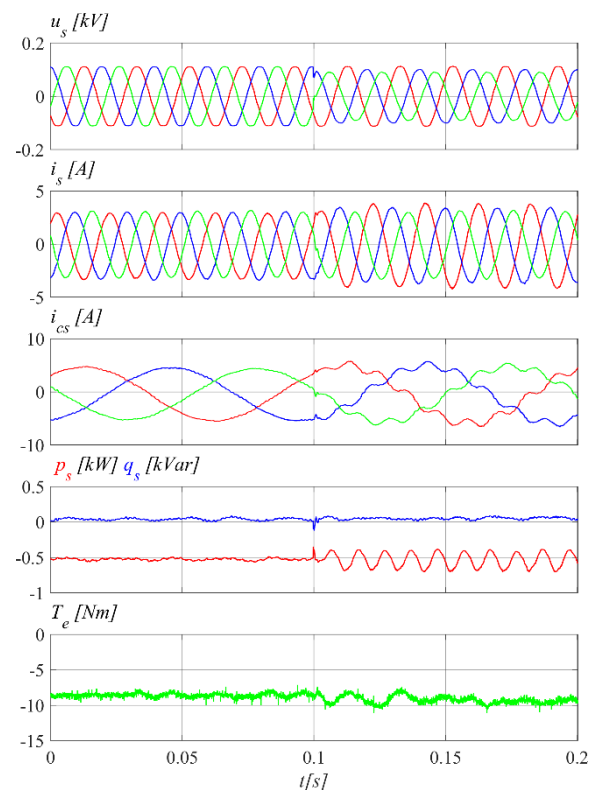


Fig. 18. Grid phase voltages u_{sa} , u_{sb} , u_{sc} ; main stator phase currents i_{sa} , i_{sb} , i_{sc} ; control stator phase currents i_{csa} , i_{csb} , i_{csc} ; active p_s and reactive q_s power components, electromagnetic torque T_e , for indirect torque control at instant grid voltage imbalance under electromagnetic torque oscillation reduction strategy.

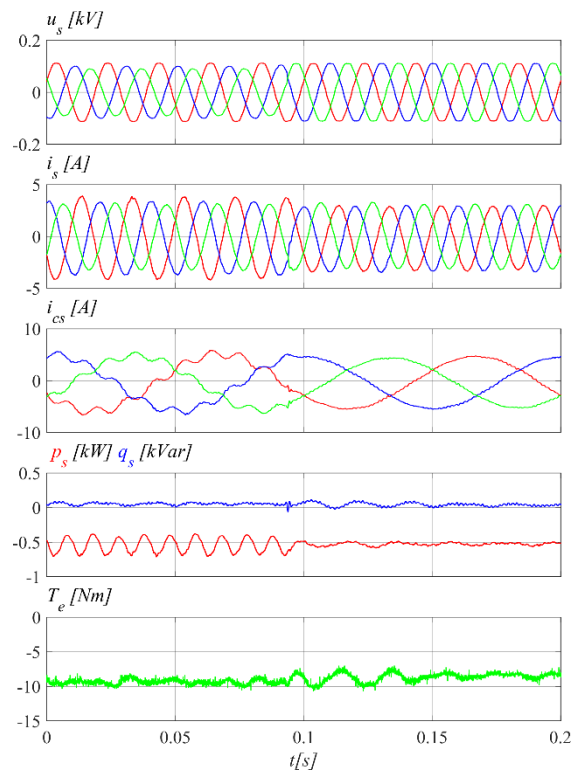


Fig. 19. Grid phase voltages u_{sa} , u_{sb} , u_{sc} ; main stator phase currents i_{sa} , i_{sb} , i_{sc} ; control stator phase currents i_{csa} , i_{csb} , i_{csc} ; active p_s and reactive q_s power components, electromagnetic torque T_e , for indirect torque control at voltage balance resumption under electromagnetic torque oscillation reduction strategy.

VI. CONCLUSIONS

The indirect torque control algorithm for the cascaded brushless doubly-fed induction generator presented in this paper can be helpful for construction of a CBDFIG-based variable speed drive-train characterized by better durability in comparison to the widely used doubly-fed induction generator and enhanced possibility of work under grid voltage unbalanced conditions. The proposed control algorithm provides the possibility of reduction of electromagnetic torque oscillations, full or partial active power component oscillations reduction for the cascaded brushless doubly-fed induction generator during operation under unbalanced grid, which can impact electric power distribution grid stability, decrease the possibility of machine damage and prolong mechanical parts life span, giving better performance of the power unit.

The reader have to note, that the whole control structure has been elaborated using linear model of brushless doubly fed induction machine without taking into consideration magnetizing inductance variation depending on the magnetizing current instantaneous values. This is why, using the linear model based methods, the reference control machine current derivation based on magnetizing current calculation may be in some range inappropriate in all, positive sequence component, negative sequence component, as well as harmonics caused by magnetizing inductance variation. Thus, obtained results for constant torque target still provide some torque oscillations. However, in a large power machines, the magnetizing current is relatively smaller in comparison to the rated stator current, so the influence on uncompensated torque pulsations are expected smaller.

APPENDIX

TABLE I
PARAMETERS OF THE CONTROL MACHINE AND THE MAIN MACHINE USED IN THE SIMULATION MODEL

SYMBOL	PARAMETER	CONTROL MACHINE	MAIN MACHINE
U_{sn}	Stator rated voltage	400/690V	400/690V
I_{sn}	Rated stator current	1760A	1760A
U_{rn}	Stator/rotor turns ratio	0.34	0.34
R_s	Stator resistance	26m Ω	26m Ω
$L_{\sigma s}$	Stator leakage inductance	0.087mH	0.087mH
R_r	Rotor resistance	26m Ω	26m Ω
$L_{\sigma r}$	Rotor leakage inductance	0.087mH	0.087mH
L_m	Magnetizing inductance	2.5mH	2.5mH
p_p	Number of poles pairs	1	1

TABLE II

PARAMETERS OF THE CONTROL MACHINE AND THE MAIN MACHINE USED IN THE REAL VERIFICATION STAND

SYMBOL	PARAMETER	CONTROL MACHINE	MAIN MACHINE
U_{sn}	Stator rated voltage	220/380V	220/380V
I_{sn}	Rated stator current	4.4A	3.5A
U_{rn}	Stator/rotor turns ratio	10.857	9.5
R_s	Stator resistance	5.4 Ω	3.8 Ω
$L_{\sigma s}$	Stator leakage inductance	0.0232H	0.018H
R_r	Rotor resistance	0.83 Ω	0.67 Ω
$L_{\sigma r}$	Rotor leakage inductance	0.0232H	0.018H
L_m	Magnetizing inductance	0.437H	0.347H
p_p	Number of poles pairs	2	2

List of symbols

R_{cs} – control machine stator resistance,
 R_s – main machine stator resistance,
 R_{cr} – control machine rotor resistance,
 R_r – main machine rotor resistance,
 L_{cs} – control machine stator inductance,
 L_s – main machine stator inductance,
 L_{cm} – control machine mutual inductance,
 L_m – main machine mutual inductance,
 L_{cr} – control machine rotor inductance,
 L_r – main machine rotor inductance,
 ψ_{cs} – control machine stator flux,
 ψ_s – main machine stator flux,
 ψ_r – main machine rotor flux,
 ψ_{cr} – control machine rotor flux,
 u_r – main machine rotor voltage,
 u_{cr} – control machine rotor voltage,
 u_{cs} – control machine stator voltage,
 u_s – main machine stator voltage,
 i_{cs} – control machine stator current,
 i_s – main machine stator current,
 i_r – main machine rotor current,

i_{cr} – control machine rotor current,
 p_b – main machine pole pairs,
 p_{cb} – control machine pole pairs,
 η_{SR} – main machine stator-to-rotor transform ratio,
 η_{CSR} – control machine stator-to-rotor transform ratio,
 Ω_s – grid voltage pulsation,
 Ω_m – rotor mechanical angular speed,
 $\Omega_{\psi s}$ – main stator magnetic flux angular speed,
 $\Omega_{\psi cs}$ – control stator magnetic flux angular speed,
 $\Omega_{\psi r}$ – rotor magnetic flux angular speed,
 Θ_m – rotor mechanical angle,
 $\Theta_{\psi s}$ – main stator magnetic flux angle,
 $\Theta_{\psi cs}$ – control stator magnetic flux angle,
 $\Theta_{\psi r}$ – rotor magnetic flux angle,
 T_e – total electromagnetic torque,
 T_{me} – torque of the main machine,
 T_{ce} – torque of the control machine,
 p – total active power,
 p_s – active power of the main machine,
 p_{cs} – active power of the control power machine,
 q – total reactive power,
 q_s – reactive power of the main machine,
 q_{cs} – reactive power of the control power machine,
 P_s – main machine active power,
 P_{cs} – control machine active power,
 P_s^{ref} – main machine reference active power,
 T_{me}^{ref} – main machine reference electromagnetic torque,
 q_s^{ref} – main machine reference reactive power,
 ψ_{sa} – main machine stator flux alpha component,
 $\psi_{s\beta}$ – main machine stator flux beta component,
 ψ'_{sa} – oppositely unbalanced main machine stator flux alpha component,
 $\psi'_{s\beta}$ – oppositely unbalanced main machine stator flux beta component,
 u_{sa} – grid voltage alpha component,
 $u_{s\beta}$ – grid voltage beta component,
 u'_{sa} – oppositely unbalanced grid voltage alpha component,
 $u'_{s\beta}$ – oppositely unbalanced grid voltage beta component,
 i_{sa} – main machine stator current alpha component,
 $i_{s\beta}$ – main machine stator current beta component,
 i_{sa}^{ref} – main machine reference stator current alpha component,
 $i_{s\beta}^{ref}$ – main machine reference stator current beta component,
 i'^{+ref}_{sa} – oppositely unbalanced main machine reference stator current alpha component,
 $i'^{+ref}_{s\beta}$ – oppositely unbalanced main machine reference stator current beta component,
 i'^{+ref}_{sa} – positive alpha component of the main machine reference stator current,
 $i'^{+ref}_{s\beta}$ – positive beta component of the main machine reference stator current,
 i_{ra}^{ref} – main machine reference rotor current alpha component,
 $i_{r\beta}^{ref}$ – main machine reference rotor current beta component,
 i'^{+ref}_{ra} – positive alpha component of the main machine reference rotor current,
 $i'^{+ref}_{r\beta}$ – positive beta component of the main machine reference rotor current,
 i_{csa}^{ref} – control machine reference rotor current alpha component,
 $i_{cs\beta}^{ref}$ – control machine reference rotor current beta component,

$i_{cs\alpha}^{ref}$ – positive alpha component of the control machine reference stator current,
 $i_{cs\beta}^{ref}$ – positive beta component of the control machine reference stator current,
 $\psi_{cs\alpha}^{ref}$ – control machine reference stator flux alpha component,
 $\psi_{cs\beta}^{ref}$ – control machine reference stator flux beta component,
 $\Delta u_{cs\alpha}$ – control stator decoupling voltage alpha component,
 $\Delta u_{cs\beta}$ – control stator decoupling voltage beta component.

REFERENCES

[1] BP Energy Outlook, “BP Energy Outlook 2019 edition,” *BP Energy Outlook 2019*, vol. April, 2019.

[2] GWEC, “Gwec Report 2018,” *Glob. Wind Energy Council*, vol. 1, 2019.

[3] P. Hevia-Koch and H. Klinge Jacobsen, “Comparing offshore and onshore wind development considering acceptance costs,” *Energy Policy*, vol. 125, pp. 9–19.

[4] J. Carroll, A. McDonald, and D. McMillan, “Reliability Comparison of Wind Turbines With DFIG and PMG Drive Trains,” *IEEE Trans. Energy Convers.*, vol. 30, no. 2, pp. 663–670, 2015.

[5] O. P. Taiwo, R. Tiako, and I. E. Davidson, “Investigation of voltage unbalance in low voltage electric power distribution network under steady state mode,” *2017 IEEE 3rd Int. Conf. Electro-Technology Natl. Dev. NIGERCON 2017*, pp. 932–939.

[6] S. Ozturk, V. Fthenakis, and S. Faulstich, “Failure modes, effects and criticality analysis for wind turbines considering climatic regions and comparing geared and direct drive wind turbines,” *Energies*, vol. 11, no. 9, pp. 1–18, 2018.

[7] T. D. Strous, H. Polinder, and J. A. Ferreira, “Brushless doubly-fed induction machines for wind turbines: Developments and research challenges,” *IET Electr. Power Appl.*, vol. 11, no. 6, pp. 991–1000, 2017.

[8] C. Vasconcelos, R. Stephan, and A. Ferreira, “Study Of The Cascaded Doubly Fed Induction Machine Dynamics Under Vector Control,” *Eletrônica de Potência*, vol. 23, no. 1, pp. 39–46, 2018.

[9] T. D. Strous, U. Shipurkar, H. Polinder, and J. A. Ferreira, “Comparing the Brushless DFIM to other Generator Systems for Wind Turbine Drive-Trains,” *J. Phys. Conf. Ser.*, vol. 753, no. 11, 2016.

[10] P. Han, M. Cheng, S. Ademi, and M. Jovanovic, “Brushless doubly-fed machines: Opportunities and challenges,” *Chinese J. Electr. Eng.*, vol. 4, no. 2, pp. 1–17, 2019.

[11] S. Tohidí et al., “Low voltage ride-through of DFIG and brushless DFIG: Similarities and differences,” *Electr. Power Syst. Res.*, vol. 110, pp. 64–72, 2014.

[12] I. A. Gowaid, A. S. Abdel-Khalik, A. M. Massoud, and S. Ahmed, “Ride-through capability of grid-connected brushless cascade DFIG wind turbines in faulty grid conditions—A comparative study,” *IEEE Trans. Sustain. Energy*, vol. 4, no. 4, pp. 1002–1015, 2013.

[13] G. Iwanski and T. Luszczuk, “Control of a Doubly Fed Induction Generator at Grid Voltage Imbalance,” *Power Electron. Drives*, vol. 2, no. 2, pp. 31–48, 2017.

[14] Y. Liu, W. Xu, J. Zhu, and F. Blaabjerg, “Sensorless Control of Standalone Brushless Doubly Fed Induction Generator Feeding Unbalanced Loads in a Ship Shaft Power Generation System,” *IEEE Trans. Ind. Electron.*, vol. 66, no. 1, pp. 739–749, 2019.

[15] O. Mohammed Elbabo Mohammed, W. Xu, and Y. Liu, “Control Design of Standalone Brushless Doubly-Fed Induction Generator for Supplying Unbalanced Loads,” *2018 IEEE Energy Convers. Congr. Expo. ECCE 2018*, pp. 7369–7374, 2018.

[16] G. Dauksha and G. Iwanski, “Modified voltage oriented control of brushless doubly fed induction generator based drivetrain under grid imbalance conditions,” *2019 Fourteenth Int. Conf. Ecol. Veh. Renew. Energies*, pp. 1–7, 2019.

[17] A. Jain and R. Saravanakumar, “Comparative analysis of DSOGI-PLL adaptive frequency Loop-PLL for voltage and frequency control of PMSG-BESS based hybrid standalone WECS,” *2018 8th Int. Conf. Power Energy Syst. ICPEs 2018*, pp. 234–239, 2019.

[18] S. Shao, T. Long, E. Abdi, and R. A. McMahon, “Dynamic control of the brushless doubly fed induction generator under unbalanced operation,” *IEEE Trans. Ind. Electron.*, vol. 60, no. 6, pp. 2465–2476, 2013.

[19] R. Pal, “Comparison of the design of FIR and IIR filters for a given specification and removal of phase distortion from IIR filters,” *Int. Conf. Adv. Comput. Commun. Cont. - ICAC3’17*, vol. Jan. 2018, pp. 1–3, 2018.

[20] S. R. Sutradhar, N. Sayadat, A. Rahman, S. Munira, A. K. M. F. Haque, and S. N. Sakib, “IIR based digital filter design and performance analysis,” *2nd Int. Conf. Telecommun. Networks, TEL-NET 2017*, pp. 1–6, 2018.

[21] J. Chen, W. Zhang, B. Chen, and Y. Ma, “Improved vector control of brushless doubly fed induction generator under unbalanced grid conditions for offshore wind power generation,” *IEEE Trans. Energy Convers.*, vol. 31, no. 1, pp. 293–302, 2016.

[22] J. Hu, J. Zhu, and D. G. Dorrell, “A new control method of cascaded brushless doubly fed induction generators using direct power control,” *IEEE Trans. Energy Convers.*, vol. 29, no. 3, pp. 771–779, 2014.

[23] N. Farah, M. H. N. Talib, Z. Ibrahim, S. N. M. Isa, and J. M. Lazi, “Variable hysteresis current controller with fuzzy logic controller based induction motor drives,” *2017 7th IEEE Int. Conf. Syst. Eng. Technol. ICSET 2017 - Proc.*, no. October, pp. 122–127, 2017.

[24] X. Li et al., “A modulated model predictive control scheme for the brushless doubly fed induction machine,” *IEEE J. Emerg. Sel. Top. Power Electron.*, vol. 6, no. 4, pp. 1681–1691, 2018.

[25] R. C. D. O. Berriel, R. M. Stephan, I. E. Chabu, and A. C. Ferreira, “Brushless cascaded doubly-fed induction machine: Modeling and simulation,” *14th Brazilian Power Electron. Conf. COBEP 2017*, pp. 1–5, 2018.

[26] A. Masmoudi, G. Iwanski, and G. Abad, “Modeling and laboratory research on brushless DFIG,” *COMPEL - Int. J. Comput. Math. Electr. Electron. Eng.*, vol. 31, no. 1, pp. 248–260, 2011.

[27] S. Bian, Y. He, and H. Zhang, “Modeling and operation analysis of the cascade brushless doubly-fed machine,” *ICEMS 2001 - Proc. 5th Int. Conf. Electr. Mach. Syst.*, vol. 2, pp. 942–945, 2001.

[28] K. Protsenko and D. Xu, “Modeling and control of brushless doubly-fed induction generators in wind energy applications,” *IEEE Trans. Power Electron.*, vol. 23, no. 3, pp. 1191–1197, 2008.

[29] A. C. Ferreira, R. M. Stephan, D. B. Lima, and F. Lessa, “Operating points of a doubly fed cascaded induction machine,” *2009 Brazilian Power Electron. Conf. COBEP2009*, pp. 124–129, 2009.

[30] P. C. L. R. Teodorescu, F. Blaabjerg, M. Liserre and Abstract, “Proportional-resonant controllers and filters for grid-connected voltage-source converters,” *IEE Proc.-Electr. Power Appl.*, vol. 153, no. 5, pp. 750–762, 2006.



Gennadiy Dauksha received the M.Sc. degree in electrical engineering from Faculty of Electrical Engineering at Warsaw University of Technology (WUT), Warszawa, Poland, in 2014. In 2014 he started PhD course in Electrical Engineering at WUT. His research is concentrated on vector control in power electronics and drives.



Grzegorz Iwanski received the M.Sc. degree in automation and robotics, and the Ph.D. degree in electrical engineering from Faculty of Electrical Engineering at Warsaw University of Technology (WUT), Warszawa, Poland, in 2003 and 2005, respectively. Since January 2006 to December 2008 he was a research worker in the Institute of Control and Industrial Electronics of WUT involved in international project within 6th Framework Programme of EU. Since 2009 he has been an Assistant Professor in Institute of Control and Industrial Electronics WUT; where in 2019 he received Associate Professor position. He teaches courses on power electronics, drives and power conversion systems. His research interests include variable and adjustable speed power generation systems, photovoltaic and energy storage systems, automotive power electronics and drives. In 2012/2013 he joined the team of REES UPC, Barcelona–Terrassa, within the framework of scholarship of Polish Minister of Science and Higher Education for investigation of power converters topologies with reduced common-mode component for photovoltaic systems. He is co-author of one monograph, three books chapters, and about 60 journal and conference papers. He provided two plenary lectures on IEEE technically sponsored international conferences (EVER’15 and OPTIM-ACEMP’17).